Double-Λ microscopic model for entangled light generation by four-wave mixing

Q. Glorieux,* R. Dubessy, S. Guibal, L. Guidoni, J.-P. Likforman, and T. Coudreau
Laboratoire Matériaux et Phénomènes Quantiques, Unité Mixte de Recherche 7162, Université Paris-Diderot CNRS 10, rue A. Domon et L. Duquet, FR-75013 Paris, France

E. Arimondo
Istituto Nazionale di Ottica, Consiglio Nazionale delle Ricerche, Dipartimento di Fisica E. Fermi, Università di Pisa, Largo Pontecorvo 3, IT-56127 Pisa, Italy

(Received 9 July 2010; published 17 September 2010)

Motivated by recent experiments, we study four-wave-mixing in an atomic double-Λ system driven by a far-detuned pump. Using the Heisenberg-Langevin formalism, and based on the microscopic properties of the medium, we calculate the classical and quantum properties of seed and conjugate beams beyond the linear amplifier approximation. A continuous-variable approach gives us access to relative-intensity noise spectra that can be directly compared with experiments. Restricting ourselves to the cold-atom regime, we predict the generation of quantum-correlated beams with a relative-intensity noise spectrum well below the standard quantum limit (down to −6 dB). Moreover, entanglement between seed and conjugate beams measured by an inseparability down to 0.25 is expected. This work opens the way to the generation of entangled beams by four-wave mixing in a cold-atom sample.

DOI: 10.1103/PhysRevA.82.033819 PACS number(s): 42.50.Ct, 42.50.Gy, 42.50.Lc

I. INTRODUCTION

Four-wave mixing (FWM) was identified early on as a very efficient process to generate intense, nonclassical beams [1]. Indeed, the first experimental demonstration of squeezed light was made using FWM in a sodium atomic beam almost 25 years ago [2]. More recently, FWM in three-level Λ systems was predicted to generate squeezing by using a counterpropagating geometry [3–6]. In addition electromagnetically induced transparency (EIT) in double-Λ atomic systems adds flexibility to the control of the FWM process, leading to large parametric gain and oscillations [7,8]. With such a system, van der Wal *et al.* generated intensity correlations between light pulses with a corresponding 0.2 dB of noise reduction below the standard quantum limit (SQL) [9]. FWM in a double-Λ system in a hot rubidium vapor and with a copropagating laser geometry was implemented in Refs. [10–15] and by some of us in Ref. [16] to generate bright correlated beams with a high degree of intensity correlations.

In order to produce paired photons or twin beams tuned near an atomic resonance, efficient FWM in atomic samples with a low parametric gain requires large optical depths. On the other hand, cold-atom samples provide a precise control of atomic parameters as inhomogeneities and decoherence processes. Thus, the combination of double-Λ EIT and cold atoms has allowed the observation of FWM at ultralow optical powers. An optically thick cesium magneto-optical trap (MOT) allowed Kuzmich *et al.* [17] to generate nonclassical photon pairs with a programmable delay. Generation and control of narrow-band paired photons were demonstrated in a rubidium MOT [18–21] by reaching a high optical depth of around 60 [22]. Correlated photons were also produced by using cold atoms inside a cavity [23].

Following [24], recent publications [25–27] have theoretically explored the time correlations between photons observed in cold-atom experiments. Propagation of the generated photons through the optically thick medium and Langevin forces represent the key elements of these theoretical analyses. Following the seminal papers in [4,5,24] and the analysis of [26], we investigate the generation of quantum-correlated beams in copropagating beam geometry. This work presents a detailed theoretical treatment of FWM in an optically thick medium composed by cold atoms described by a four-level model, in a double-Λ configuration.

The main target is to explore the production of correlated beams in the atom-laser configuration experimentally investigated in Refs. [10–16], but using a cold-atom sample as in Refs. [19–22]. While the theoretical descriptions [25–27] concentrated on the few photon regime, the experiments discussed in Refs. [10–16] require one to tackle the large photon number regime where a description based on continuous variables is required [28,29]. Within this approach, we derive the quantum noise frequency spectra and quantify the quantum entanglement between the generated beams.

Several additional original points of our analysis should be listed. First, we investigate the pump-seed copropagating geometry, a setup which enabled us to produce large-intensity quantum correlations in the experiments [10–16]. Furthermore, in contrast to the phenomenological description of Ref. [12], gain and propagation losses are intrinsically included in our microscopic approach. As the most important result, our analytical and numerical analysis predicts that a very large degree of intensity quantum correlation can be achieved also in a cold-atom FWM experiment, comparable to that achieved in Refs. [10,11,16]. We also investigate the ability of such a medium to simultaneously generate large phase anticorrelations, leading to entanglement, a key resource for quantum information [29].

The paper is organized as follows. Section II introduces the microscopic model as described by Heisenberg-Langevin equations. Section III discusses the analytical solution for the propagating quantum fields. In Sec. IV we derive the mean

*quentin.glorieux@univ-paris-diderot.fr

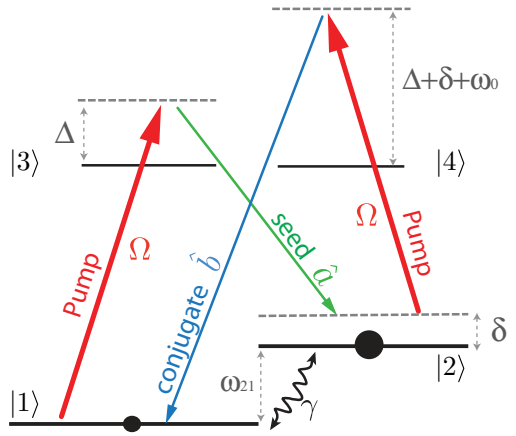

FIG. 1. (Color online) Level diagram with relevant detunings. The two large red arrows indicate the pump coupling between levels $|1\rangle$ and $|3\rangle$ (respectively, $|2\rangle$ and $|4\rangle$), with equal Rabi frequency Ω. δ represents the two-photon detuning on both Λ subsystems. The strong pump and weak seed configuration leads to optical pumping of the atoms into level $|2\rangle$.

values of the generated beams. We introduce and calculate in Sec. V the intensity quantum correlation and phase quantum anticorrelation spectra between seed and conjugate beams including the Langevin forces contribution. Finally, in Sec. VI, we discuss the effect of decoherence processes and compare the results with those from hot-vapor experiments.

II. MICROSCOPIC MODEL—LANGEVIN EQUATIONS

We consider a collection of atoms having the double-Λ-type four-level scheme of Fig. 1. The four atomic levels $|u\rangle$ are defined by their energies E_u, and we introduce the angular frequencies $\omega_{uv} = (E_u - E_v)/\hbar$, where $u,v \in \{1,2,3,4\}$, $u > v$. The populations of levels $|3\rangle$ and $|4\rangle$ decay with a rate Γ. The atomic coherence between levels $|1\rangle$ and $|2\rangle$ decays with rate γ and we neglect $|1\rangle$ and $|2\rangle$ population decays since we consider cold-atom samples.

The atoms interact with three optical fields, pump (angular frequency ω_p) and seed (angular frequency ω_a) driving the first Λ subsystem ($|1\rangle \rightarrow |3\rangle \rightarrow |2\rangle$), and conjugate (angular frequency ω_b) and pump driving the second Λ subsystem ($|1\rangle \rightarrow |4\rangle \rightarrow |2\rangle$). The detuning of the pump field from the $|1\rangle \rightarrow |3\rangle$ transition is denoted Δ. The pump and the seed are near-resonant with the $|1\rangle \rightarrow |3\rangle \rightarrow |2\rangle$ Raman transition with a two-photon detuning δ. The double Λ is closed by the conjugate and pump beams driving the $|1\rangle \rightarrow |4\rangle \rightarrow |2\rangle$ Raman transition, assuming energy matching. As shown in Fig. 1, the pump laser is detuned by $\Delta + \omega_0 + \delta$ from the $|2\rangle \rightarrow |4\rangle$ transition, where $\omega_0 = \omega_{21} - \omega_{43}$.

The interactions of the pump beam with the atoms are described semiclassically. For the sake of simplicity, we limit our study to a one-dimensional model with propagation along the z axis. The seed and conjugate beams are described by two slowly varying quantum-mechanical operators; the annihilation (creation) operators being denoted $\hat{a}$ ($\hat{a}^\dagger$) and $\hat{b}$ ($\hat{b}^\dagger$).

Following the approach of Ref. [24], the properties of the medium are described by collective, slowly varying operators $\hat{\sigma}_{uv}(z,t)$ averaged over small layers denoted by their position z. For each layer containing a large number of atoms N_z, we define the following population and coherence operators $\hat{\sigma}_{uv}$:

$$\hat{\sigma}_{uv}(z,t) = \frac{1}{N_z}\sum_{j=1}^{N_z} |u_j\rangle\langle v_j| e^{(-i\tilde{\omega}_{uv}t + ik_{uv}z)}, \tag{1}$$

where $\tilde{\omega}_{31} = \tilde{\omega}_{42} = \omega_p$, $\tilde{\omega}_{32} = \omega_a$, $\tilde{\omega}_{41} = \omega_b$, and $\tilde{\omega}_{21} = \tilde{\omega}_{43} = \omega_p - \omega_a$. The k_{uv} are the projections of the wave vectors $\vec{k}_{uv}$ on the z axis with $\vec{k}_{31}$ and $\vec{k}_{42}$ equal to the pump wave vector, $\vec{k}_{32}$ equal to the seed wave vector, and $\vec{k}_{41}$ equal to the conjugate wave vector, $\vec{k}_{21} = \vec{k}_{23} - \vec{k}_{13}$ and $\vec{k}_{43} = \vec{k}_{42} - \vec{k}_{32}$, with the convention $\vec{k}_{uv} = -\vec{k}_{vu}$.

We write the laser-atom interaction Hamiltonian $\hat{V}$ in the rotating wave approximation, omitting for simplicity the z and t dependencies of the atomic operators:

$$\hat{V} = -\frac{\hbar N}{L}\int_0^L dz \Big[(\omega_0 + \Delta + \delta)\,\hat{\sigma}_{44} + \Delta\hat{\sigma}_{33} + \delta\hat{\sigma}_{22} + g_a\hat{a}(z,t)\hat{\sigma}_{32} + g_b\hat{b}(z,t)\hat{\sigma}_{41} + \frac{\Omega}{2}(\hat{\sigma}_{31} + \hat{\sigma}_{42})\Big] + \text{H.c.}, \tag{2}$$

where N is the number of atoms in the quantization volume V of length L. $g_{a,b}$ are the atom-field coupling constants: $g_a = \frac{\wp_{32}\varepsilon_a}{\hbar}$ and $g_b = \frac{\wp_{41}\varepsilon_b}{\hbar}$ where $\wp_{uv}$ is the transition dipole moment, and $\varepsilon_{a,b} = \sqrt{\frac{\hbar\,\omega_{a,b}}{2\epsilon_0 V}}$ is the electric field of a single photon. In the following, we consider $g_a = g_b = g$. Finally, $\Omega = \frac{2\wp E}{\hbar}$ is the pump laser Rabi frequency with E the pump laser electric field amplitude. We assume the transition dipole moment $\wp$ to be equal for the two pump-driven transitions $|1\rangle \rightarrow |3\rangle$ and $|2\rangle \rightarrow |4\rangle$.

As described in Ref. [26], the evolution of atomic operators is determined by the following Heisenberg-Langevin equations:

$$\left(\frac{\partial}{\partial t} + \gamma_{uv}\right)\hat{\sigma}_{uv} = \frac{i}{\hbar}[\hat{V},\hat{\sigma}_{uv}] + \hat{r}_{uv} + \hat{F}_{uv}, \tag{3}$$

where γ_{uv} are the atomic dephasing rates and $\hat{r}_{uv}$ are the source terms produced by spontaneous emission as defined in [26]. Following Ref. [25], the Langevin operators $\hat{F}_{uv}$ are characterized by

$$\langle\hat{F}_{uv}(z,t)\rangle = 0, \tag{4}$$

and

$$\langle\hat{F}^\dagger_{uv}(z,t)\hat{F}_{u'v'}(z',t')\rangle = 2D_{uv,u'v'}\delta(t-t')\delta(z-z'). \tag{5}$$

Equation (5) defines the 256 diffusion coefficients $D_{uv,u'v'}$; we show in Appendix B that only a few of them will be required in the next section.

Following the approach of Refs. [5,7,26], the description of the atom-laser system is completed by a set of nonlinear, coupled differential equations describing the propagation and temporal evolution of the quantum field operators

$$\left(\frac{\partial}{\partial t} + c\frac{\partial}{\partial z}\right)\hat{a}(z,t) = ig\mathcal{N}\hat{\sigma}_{23}(z,t), \tag{6}$$

$$\left(\frac{\partial}{\partial t} + c\frac{\partial}{\partial z}\right)\hat{b}^\dagger(z,t) = -ig\mathcal{N}\hat{\sigma}_{41}(z,t), \tag{7}$$

where $\mathcal{N} = N/V$ is the atomic density.

III. ANALYTICAL SOLUTION

The system evolution is described by a set of nonlinear, coupled differential equations for quantum fields and atomic operators which require further approximations to be solvable analytically. We assume a pump beam highly saturating the medium and very intense compared to the seed and conjugate beams. Within these assumptions the populations $\hat{\sigma}_{11},\hat{\sigma}_{22},\hat{\sigma}_{33},\hat{\sigma}_{44}$ and the coherences $\hat{\sigma}_{31},\hat{\sigma}_{13},\hat{\sigma}_{42},\hat{\sigma}_{24}$ are dominantly driven by the pump beam. In this case the complete nonlinear differential equation system can be separated into two subsystems. In the first subsystem [Eq. (A1)], the effect of seed and conjugate can be neglected and these equations are solved in the steady state. The corresponding solutions are given in Appendix A. These solutions are then injected into Eq. (B1), which determines the coherences $\hat{\sigma}_{14},\hat{\sigma}_{41},\hat{\sigma}_{23},\hat{\sigma}_{32},\hat{\sigma}_{12},\hat{\sigma}_{21},\hat{\sigma}_{34},\hat{\sigma}_{43}$ as a function of $\hat{a}$ and $\hat{b}^\dagger$ as described in detail in Appendix B.

Equations (6) and (7) can then be written in a closed form and solved analytically in the Fourier space. The Fourier transforms of $\hat{a}(t,z),\hat{b}^\dagger(t,z)$ will be denoted $\hat{a}(\omega,z),\hat{b}^\dagger(\omega,z)$, where for simplicity we have used the same notation for operators in the time and frequency domains.

Notice our notation for the Fourier transform of an operator and its conjugate

$$\hat{a}(\omega)=\int_{-\infty}^{\infty}\hat{a}(t)\,e^{i\omega t}\,dt,\quad \hat{a}^\dagger(\omega)=\int_{-\infty}^{\infty}\hat{a}^\dagger(t)\,e^{i\omega t}\,dt, \tag{8}$$

leading to $[\hat{a}(\omega)]^\dagger=\hat{a}^\dagger(-\omega)$. The Fourier transforms of the quantum operators satisfy then the following equations:

$$\frac{1}{k_{32}}\frac{\partial}{\partial z}\hat{a}(\omega)=\eta_a(\omega)\hat{a}(\omega)+\kappa_a(\omega)\hat{b}^\dagger(\omega)+\hat{\mathcal{F}}_a^{\rm at}(\omega), \tag{9}$$

$$\frac{1}{k_{41}}\frac{\partial}{\partial z}\hat{b}^\dagger(\omega)=\kappa_b(\omega)\hat{a}(\omega)+\eta_b(\omega)\hat{b}^\dagger(\omega)+\hat{\mathcal{F}}_{b^\dagger}^{\rm at}(\omega), \tag{10}$$

where $\eta_a(\omega)$ $[\eta_b(\omega)]$ is the complex refractive index of the medium "dressed" by the pump laser for the mode $\hat{a}$ $(\hat{b}^\dagger)$. $\kappa_a(\omega)$ $[\kappa_b(\omega)]$ is the parametric conversion coefficient from mode $\hat{a}$ to $\hat{b}^\dagger$ ($\hat{b}^\dagger$ to $\hat{a}$), and $\hat{\mathcal{F}}_a^{\rm at}$ and $\hat{\mathcal{F}}_{b^\dagger}^{\rm at}$ are the Langevin terms originating from the atomic Langevin forces and can be calculated from Eq. (B10).

Following a standard approach of quantum optics [30], we use the input-output formalism to compute the quantum operators of seed and conjugate fields. We introduce the input operators, $\hat{a}_{\rm in}$ and $\hat{b}_{\rm in}^\dagger$ for $z=0$ and the output operators $\hat{a}_{\rm out}$ and $\hat{b}_{\rm out}^\dagger$ for $z=L$. The formal solution of the propagation Eqs. (9) and (10) is given by

$$\begin{bmatrix}\hat{a}_{\rm out}(\omega)\\ \hat{b}_{\rm out}^\dagger(\omega)\end{bmatrix}=\begin{bmatrix}A(\omega) & B(\omega)\\ C(\omega) & D(\omega)\end{bmatrix}\left(\begin{bmatrix}\hat{a}_{\rm in}(\omega)\\ \hat{b}_{\rm in}^\dagger(\omega)\end{bmatrix}+\begin{bmatrix}\hat{F}_{a,{\rm out}}(\omega)\\ \hat{F}_{b,{\rm out}}(\omega)\end{bmatrix}\right), \tag{11}$$

for which the coefficients $A(\omega)$, $B(\omega)$, $C(\omega)$, and $D(\omega)$ and the Langevin terms $\hat{F}_{b,{\rm out}}(\omega)$ and $\hat{F}_{a,{\rm out}}(\omega)$ are defined in Appendix C. Equation (11) allows us to compute both the output field mean values $(\langle\hat{a}_{\rm out}\rangle,\langle\hat{b}_{\rm out}^\dagger\rangle)$ and their fluctuations $(\delta\hat{a}_{\rm out},\delta\hat{b}_{\rm out}^\dagger)$.

As in typical FWM experiments, in the following we will suppose that the input on the conjugate mode $\hat{b}$ is the vacuum $(\langle\hat{b}_{\rm in}\rangle=0)$ and that the input on the seed mode is an arbitrary field of mean value $\langle\hat{a}_{\rm in}\rangle$. The average values of the output seed and conjugate fields are given by

$$\langle\hat{a}_{\rm out}(\omega=0)\rangle=A(0)\langle\hat{a}_{\rm in}\rangle, \tag{12}$$

$$\langle\hat{b}_{\rm out}^\dagger(\omega=0)\rangle=C(0)\langle\hat{a}_{\rm in}\rangle. \tag{13}$$

We define then $G_a=|A(0)|^2$ as the seed gain, and $G_b=|C(0)|^2$ as the ratio between the conjugate output and seed input intensities.

IV. CLASSICAL PROPERTIES OF THE MEDIUM

The mean value expressions for the seed and conjugate output operators allow us to calculate the output intensities which can be experimentally measured. The parameters used in the following for laser intensities and detunings are derived from hot-vapor experiments such as in [10–16], so that in our numerical calculations, we will use $0.7<\Delta/2\pi<3$ GHz and $0.3<\Omega/2\pi<2$ GHz.

We consider the D_1 transition of ^{85}Rb: lasers wavelength 795 nm; $\omega_0/2\pi=3$ GHz; natural linewidth $\Gamma/2\pi=5.7$ MHz; resonant absorption cross section $\sigma_0=10^{-9}$ cm^2 [31]. For the optical depth defined by $\mathcal{N}\sigma_0 L$, we use the value of 150 reachable by improving a cold-atom configuration such that of Ref. [22]. In cold-atom experiments, magnetic-field inhomogeneity and atomic collisions may determine the γ decoherence rate. In a state-of-the-art experiment, γ depends mainly on the relative phase stability of the lasers and is as low as $\gamma/2\pi\simeq 10$ Hz [32]. However, as specifically discussed in Sec. VI A, our results shows a weak dependence on this parameter, and $\gamma/2\pi=10$ kHz will be usually assumed.

Figure 2 reports numerical simulation results for the seed and conjugate gains as functions of the two-photon detuning δ. As described in Ref. [6], different elementary processes contribute to the system dynamics. Effective coherent photon redistribution from pump to seed and conjugate occurs when the four-photon resonance condition is fulfilled ($\delta\simeq 0$). Let us note that the same resonance condition holds for a Raman absorption process involving the seed beam. While it is quite obvious that mode $\hat{b}$ will always be amplified as soon as the nonlinearity exceeds the absorption loss, the behavior of mode $\hat{a}$ is more complicated and relies on the interference between redistribution and Raman processes. The spectrum profile of the seed gain [Fig. 2(a)] is characterized by absorption at $\delta\simeq\Delta$, with a width imposed by Γ and the propagation through the optically thick medium. For $\delta\simeq 0$, the seed gain spectrum displays a sharp profile containing both gain and absorption contributions [Fig. 2(a) inset]. The seed absorption is due to the Raman process on the transition $|2\rangle\rightarrow|1\rangle$ involving one seed photon and one pump photon, while the gain can be attributed to the FWM process. For a pump laser in resonance with one "arm" of the Λ transition, the EIT profile assumes the characteristic line shape of a narrow dip inside a Lorentzian profile. In an EIT configuration with the pump laser detuned from the resonance, the absorption profile of the seed field becomes asymmetric about the two-photon resonance assuming a characteristic Fano-like profile as in the experiments of Refs. [33–36] and the theoretical analysis of Ref. [37]. The $\delta\simeq 0$ profile of G_a is similar to the EIT Fano

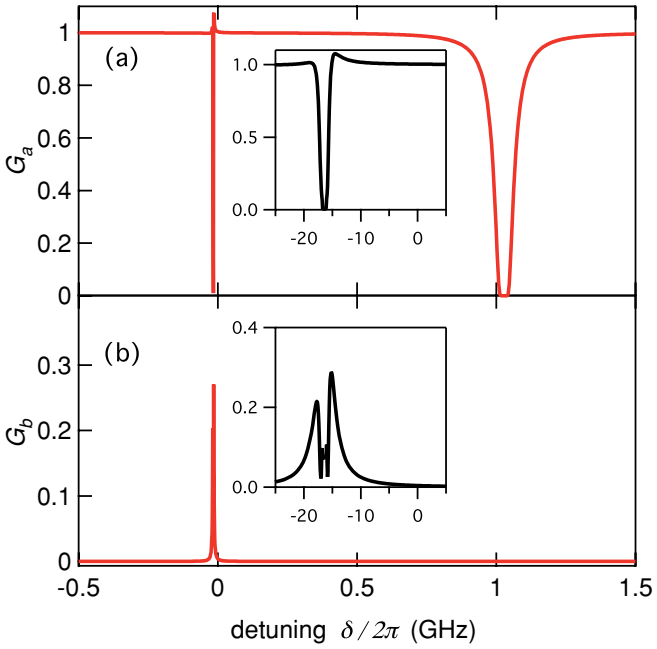

FIG. 2. (Color online) Spectra of (a) the G_a seed beam gain and (b) the conjugate beam gain G_b as functions of the two-photon detuning δ. The parameters used for the plot are $\gamma/2\pi = 10$ kHz; $\Omega/2\pi = 0.3$ GHz; $\Delta/2\pi = 1$ GHz. The seed beam dip for $\delta \simeq \Delta$ in (a) is originated by absorption on the $|2\rangle \rightarrow |3\rangle$ transition. Expanded views of G_a and G_b gains around $\delta = 0$ are shown in the insets. The peculiar line shapes are the result of a nontrivial interplay between the two processes discussed in the text.

profiles reported in the above references, except that $G_a \geqslant 1$ in a narrow frequency range. The precise positions of the seed absorption and Fano-like feature are given by the ac Stark shifts induced by the pump laser.

The G_b spectrum, shown in Fig. 2(b), reports a reduction of the gain in the region $\delta \simeq 0$ with a width matching that of the dip in the G_a spectrum. In a naive description, conjugate gain does not increase along the propagation when the seed is completely depleted.

V. QUANTUM PROPERTIES OF THE SYSTEM

A. Noise spectra

Now we focus our attention on the quantum properties of the system. We follow the standard approach of the continuous-variable formalism [30] to calculate the noise spectra. For the seed mode $\hat{a}$ we introduce the following amplitude and phase quadrature fluctuation components, $\delta\hat{x}_a$ and $\delta\hat{p}_a$, respectively:

$$\delta\hat{x}_a = \delta\hat{a}e^{-i\varphi_a} + \delta\hat{a}^\dagger e^{i\varphi_a}, \tag{14}$$

$$\delta\hat{p}_a = -i(\delta\hat{a}e^{-i\varphi_a} - \delta\hat{a}^\dagger e^{i\varphi_a}), \tag{15}$$

where φ_a is the phase of the mean field $\langle\hat{a}\rangle$. We define accordingly the amplitude quadrature fluctuations for the conjugate mode $\hat{b}$, $\delta\hat{x}_b$ and $\delta\hat{p}_b$. Following the Wiener-Khintchine theorem, the spectrum of a given quantity $\hat{u}$ can be evaluated by taking the Fourier transform of its autocorrelation function [30]:

$$S_{\hat{u}}(\omega)2\pi\delta(\omega - \omega') = \langle\hat{u}(\omega)\hat{u}^\dagger(\omega')\rangle. \tag{16}$$

We analyze the FWM configuration of Refs. [10–16] with a coherent state for the seed input of mean value amplitude α. In agreement with the symmetric ordering of the operators [30] to be used hereafter, the covariance matrix for the input seed field is given by

$$\begin{bmatrix} \langle\delta\hat{x}_{a,\mathrm{in}}(\omega)\delta\hat{x}^\dagger_{a,\mathrm{in}}(\omega')\rangle & \langle\delta\hat{x}_{a,\mathrm{in}}(\omega)\delta\hat{p}^\dagger_{a,\mathrm{in}}(\omega')\rangle \\ \langle\delta\hat{p}_{a,\mathrm{in}}(\omega)\delta\hat{x}^\dagger_{a,\mathrm{in}}(\omega')\rangle & \langle\delta\hat{p}_{a,\mathrm{in}}(\omega)\delta\hat{p}^\dagger_{a,\mathrm{in}}(\omega')\rangle \end{bmatrix} = 2\pi\delta(\omega + \omega')\begin{bmatrix} 1 & 0 \\ 0 & 1 \end{bmatrix}, \tag{17}$$

and a similar definition applies for covariance matrix of the conjugate mode but with a zero mean input power. Notice that, according to [38,39], the choice of ordering of the operators should not influence the calculated spectra.

Using Eq. (11) for the propagation of the quantum operators for the seed and conjugate fields and the input covariance matrix defined in Eq. (17), the quantum noise spectra for the quadrature amplitude of the fields are given by

$$\begin{aligned} S_{\hat{x}_{a,\mathrm{out}}}(\omega) = \frac{|\langle\hat{a}_{\mathrm{out}}\rangle|^2}{2}\{&|A(\omega)|^2[1 + D_{aa^\dagger}(\omega)] \\ &+ |A(-\omega)|^2[1 + D_{a^\dagger a}(-\omega)] \\ &+ |B(\omega)|^2[1 + D_{b^\dagger b}(\omega)] \\ &+ |B(-\omega)|^2[1 + D_{bb^\dagger}(-\omega)]\}, \end{aligned} \tag{18}$$

$$\begin{aligned} S_{\hat{x}_{b,\mathrm{out}}}(\omega) = \frac{|\langle\hat{b}_{\mathrm{out}}\rangle|^2}{2}\{&|C(\omega)|^2[1 + D_{aa^\dagger}(\omega)] \\ &+ |C(-\omega)|^2[1 + D_{a^\dagger a}(-\omega)] \\ &+ |D(\omega)|^2[1 + D_{b^\dagger b}(\omega)] \\ &+ |D(-\omega)|^2[1 + D_{bb^\dagger}(-\omega)]\}, \end{aligned} \tag{19}$$

where the calculation method of the four atom-driven Langevin diffusion terms $D_{aa^\dagger}$, $D_{a^\dagger a}$ $D_{b^\dagger b}$, and $D_{bb^\dagger}$ is presented in Appendix D. All those coefficients are, by construction, real and positive quantities and act as additional noise source terms on the quantum noise spectra. Their specific contribution will be discussed below.

The interest in the double-Λ FWM system stems in particular from its ability to generate quantum field correlations. Such correlations can concern a single quadrature of seed and conjugate fields (e.g., intensity correlations as in Refs. [40,41]) or two conjugated quadratures (e.g., intensity correlations and phase anticorrelations). In the second case, seed and conjugate fields can be entangled. Let us note that while most FWM experiments have investigated intensity squeezing, Ref. [14] reports entanglement in a hot atomic vapor. In order to detect the entanglement, we will here use the $\mathcal{I}(\omega) < 1$ sufficient criterion introduced in [42,43] and, based on the inseparability parameter, defined by

$$\mathcal{I}(\omega) = \tfrac{1}{2}(S_x^- + S_p^+). \tag{20}$$

Here S_x^- is the intensity correlation spectrum and S_p^+ the phase anticorrelation spectrum both normalized to the standard quantum limit (SQL). S_x^- is derived by applying Eq. (16) to

$$\hat{u} = \frac{1}{\sqrt{2}}[\delta\hat{x}_{a,\mathrm{out}}(\omega) - \delta\hat{x}_{b,\mathrm{out}}(\omega)] \tag{21}$$

and normalizing it to the sum of gain on mode $\hat{a}$ and mode $\hat{b}$: $(G_a + G_b)$. Correspondingly S_p^+ is obtained with

$$\hat{u} = \frac{1}{\sqrt{2}}[\delta\hat{p}_{a,\mathrm{out}}(\omega) + \delta\hat{p}_{b,\mathrm{out}}(\omega)], \tag{22}$$

with the same normalization. Inseparability will be used below to give a higher bound for entanglement as discussed in Ref. [44]. Equation (20) leads to the following expressions for the normalized intensity correlation spectrum and the normalized phase anticorrelation spectrum:

$$\begin{aligned} S_x^-(\omega) = \frac{1}{2(G_a+G_b)}\{&[|A(0)^*A(\omega) - C(0)^*C(\omega)|^2] \\ &\times [1 + D_{aa^\dagger}(\omega)] + [|A(0)A(-\omega)^* - C(0)C(-\omega)^*|^2] \\ &\times [1 + D_{a^\dagger a}(-\omega)] + [|A(0)^*B(\omega) - C(0)^*D(\omega)|^2] \\ &\times [1 + D_{b^\dagger b}(\omega)] + [|A(0)B(-\omega)^* - C(0)D(-\omega)^*|^2] \\ &\times [1 + D_{bb^\dagger}(-\omega)]\}, \end{aligned} \tag{23}$$

$$\begin{aligned} S_p^+(\omega) = \frac{1}{2(G_a+G_b)}\{&[|A(0)C(\omega) - C(0)^*A(\omega)^*|^2] \\ &\times [1 + D_{aa^\dagger}(\omega)] + [|A(0)C(-\omega)^* \\ &- C(0)^*A(-\omega)^*|^2][1 + D_{a^\dagger a}(-\omega)] \\ &+ [|A(0)D(\omega) - C(0)^*B(\omega)^*|^2][1 + D_{b^\dagger b}(\omega)] \\ &+ [|A(0)D(-\omega)^* - C(0)^*B(-\omega)^*|^2] \\ &\times [1 + D_{bb^\dagger}(-\omega)]\}. \end{aligned} \tag{24}$$

In contrast to the case of Eq. (18), which is a sum of positive terms, a nonvanishing set of coefficients A, B, C, D could exist in Eq. (23), such that the spectrum of the intensity difference $S_x^-(\omega) \to 0$ [the same holds for Eq. (24)]. For example, in the case of a system behaving as an infinite bandwidth ideal linear amplifier having gain equal to G [$|A(\omega)|^2 = |D(\omega)|^2 = G$ and $|B(\omega)|^2 = |C(\omega)|^2 = G - 1$, and vanishing D_{uv}], the relative-intensity noise spectra is given by

$$S_x^-(\omega) = \frac{1}{2G-1}, \tag{25}$$

as reported in [12]. Let us note that our model describes the frequency dependence of the noise spectra as well as the Langevin forces contribution through the coefficients $D_{aa^\dagger}$, $D_{a^\dagger a}$, $D_{b^\dagger b}$, and $D_{bb^\dagger}$.

Figure 3 displays the intensity correlation and phase anticorrelation spectra versus $\omega/2\pi$ (analysis frequency) for two values of Ω and Δ. For each set of values, the two-photon detuning δ is chosen in order to optimize the noise reduction, close to the maximum gain value. In both cases the output beams are entangled, since they display both nonclassical intensity correlations and phase anticorrelations. Our calculation shows that, within the explored range of parameters, at fixed Ω/Δ the optimum entanglement increases with Ω. Let us note that both seed and conjugate output beams display an intensity noise above the standard quantum limit as reported in hot-atomic-vapor experiments [10].

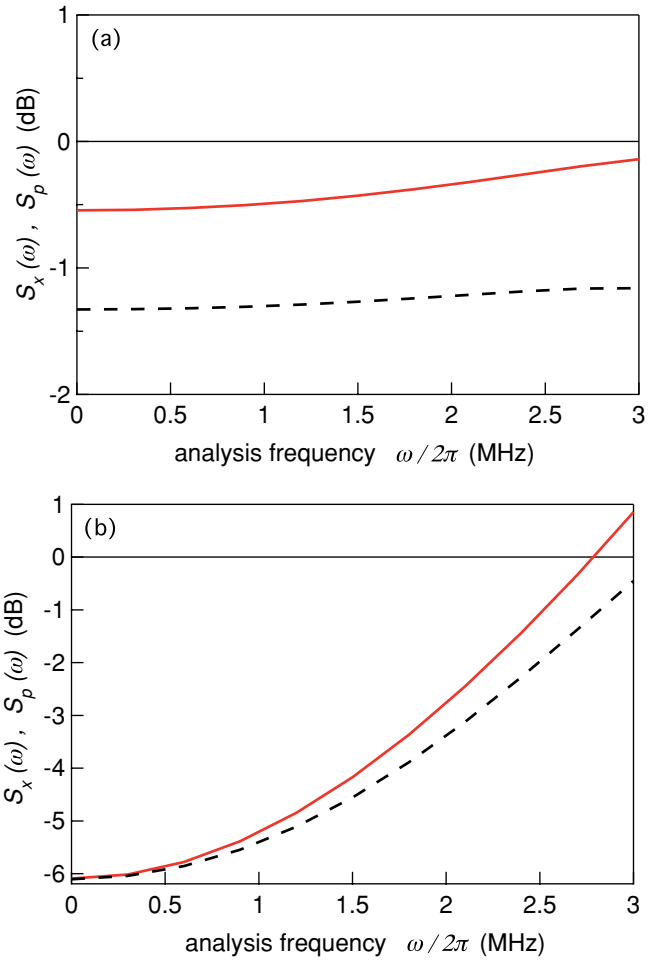

FIG. 3. (Color online) Intensity correlation (black dashed) and phase anticorrelation (red continuous) spectra (in dB) as functions of analysis frequency for (a) $\Omega/2\pi = \Delta/2\pi = 0.3$ GHz and $\delta/2\pi = -48$ MHz and (b) $\Omega/2\pi = \Delta/2\pi = 2$ GHz and $\delta/2\pi = -217$ MHz. Inseparability can be obtained by taking the half sum of the two correlation spectra.

B. Contribution of Langevin forces

Equations (23) and (24) show that the contribution of the Langevin forces is purely detrimental to entanglement. In a previous paper studying similar systems [26], the contribution of Langevin forces was negligible. In our system we found that it was not the case, and we have specifically investigated their role. Figure 4 shows the inseparability spectra versus the analysis frequency in the presence and absence of the Langevin terms. Their effect is small but clearly non-negligible and increases with ω. Let us point out that when neglecting the Langevin correction terms, our calculation leads to nonphysical spectra for the mode $\hat{a}$, i.e., the noise can fall simultaneously below the SQL for both phase and intensity quadratures. On the contrary, by including the Langevin terms, we always obtain, as mentioned above, excess noise on both quadratures.

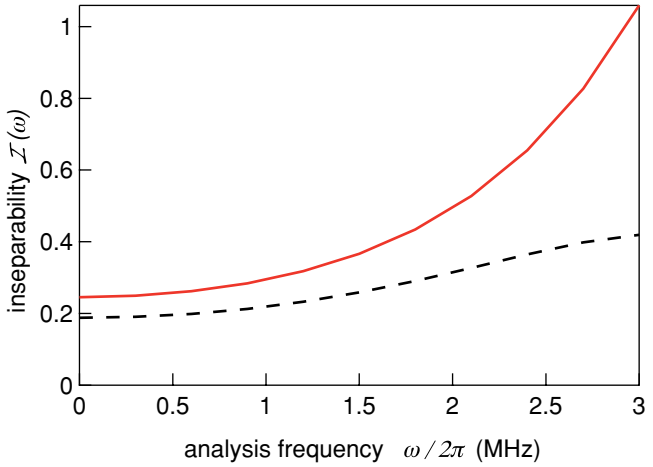

FIG. 4. (Color online) Inseparability with (red line) and without (black dashed) the Langevin noise correction. Parameters as in Fig. 3(b).

VI. DISCUSSION

Below, we discuss briefly the role of the ground-state decoherence rate as well as the comparison of the model to the results of a hot-vapor experiment.

A. Role of the ground-state decoherence rate

Quantum correlations are notably sensitive to various decoherence mechanisms. In Fig. 5, we present the evolution of the maximal quantum correlations (in terms of the $\mathcal{I}$ inseparability) as a function of the γ decoherence rate. While high relaxation rates ($\gamma/2\pi > 10$ MHz) do not allow the observation of entanglement, the smooth behavior in the low-γ region shows that the system is quite robust against mild decoherence mechanisms. These observations show that coherences between hyperfine levels play a key role in the production of entanglement in FWM experiments.

B. Comparison with hot-atomic-vapor experiments

The presented numerical results were obtained assuming a stationary regime (no transient phenomena associated with

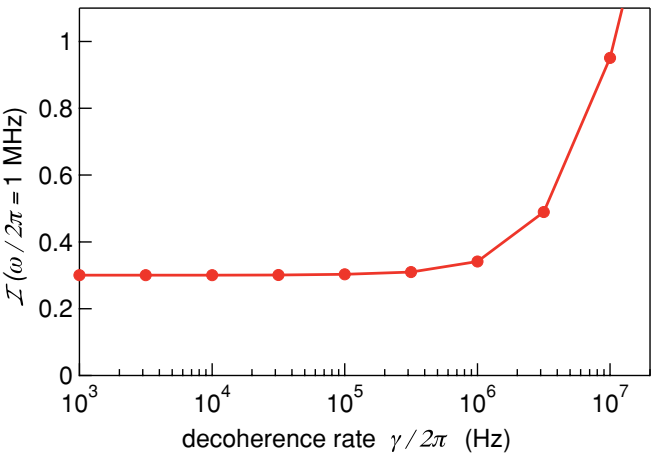

FIG. 5. (Color online) Effect of the decoherence between the two ground states on the $\mathcal{I}(\omega)$ inseparability at $\omega/2\pi = 1$ MHz. One can see that the process is robust to decoherence up to 1 MHz. Parameters: $\Omega/2\pi = \Delta/2\pi = 2$ GHz, $\delta/2\pi = -217$ MHz.

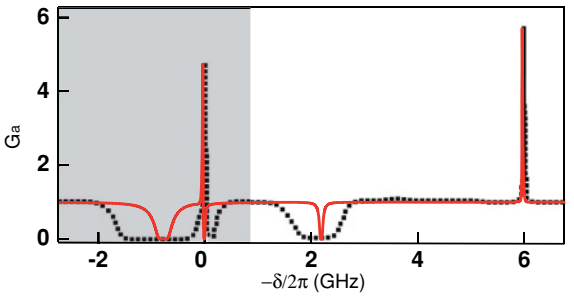

FIG. 6. (Color online) Gain spectrum G_a of a weak seed beam as a function of the two-photon detuning δ. The black dashed line reports the experimental data for a heated Rb cell [11]. These results are obtained with a pump power $P = 400$ mW, a pump beam waist of 650 μm ($\Omega/2\pi = 330$ MHz), a pump detuning $\Delta/2\pi = 700$ MHz, and $L = 12.5$ mm. The red solid line corresponds to the theoretical predictions of our model using those parameters and an atomic density $\mathcal{N} = 4 \times 10^{12}$ cm^{-3} in agreement with that estimated from the measured Rb cell temperature. The gray shaded area corresponds to the spectrum reported in Fig. 2(a) (please note the reversed scale). The absorption dip and the Fano-like profile on the right part of the figure, absent in the simulation of Fig. 2, are originated by the seed acting on the $|1\rangle \rightarrow |4\rangle$ transition.

transit time) and in the absence of inhomogeneous Doppler broadening. The extension of the model to include these effects is beyond the scope of the present work. However, let us present the result of the calculation of the G_a seed gain, using our cold-atom model, assuming the set of atom and laser parameters explored by McCormick *et al.* [10]. For the atomic density, we assume $\mathcal{N} \simeq 4 \times 10^{12}$ cm^{-3} falling into the range explored by the experiments of Refs. [10–16]. We estimate the decoherence rate $\gamma/2\pi = 500$ kHz from the mean transit time through the pump beam.

Figure 6 shows our numerical results for the G_a spectrum and compares them with the experimental observations kindly provided by P. D. Lett. Notice that the gain spectrum contains twice the absorption and Fano-like feature of Fig. 2, because the seed and conjugate beams exchange their roles in a large scan of the seed laser frequency. Even if the cold-atom model cannot reproduce exactly the data obtained in a heated cell where the Doppler effect plays a major role, the main features of the experimental transmission profile are well reproduced. In addition the gain peaks occur at the predicted two-photon detuning, the coherent absorption dips are present, and finally the asymmetric profile of the left peak is also accounted for. The gain peak values of the hot-vapor experiment are in very good agreement with those predicted by the cold-atom simulation.

VII. CONCLUSION

We explored analytically and numerically the FWM generation process for an atomic double-Λ system. The Heisenberg-Langevin formalism allowed us to describe the classical and quantum properties of seed and conjugate beams beyond the linear noiseless amplifier approximation. A continuous-variable approach gave us access to relative-intensity noise spectra (which can be directly compared with experiments). In the very wide parameter space of this system, we explored a range of large pump Rabi frequency and detuning, recently addressed by hot-Rb-vapor experiments. However, Doppler

broadening was not taken into account in our analysis, and the optical depth was assumed compatible with a cold-atom sample. In this previously unexplored regime, we predict the generation of quantum-correlated beams with a relative-intensity noise spectrum well below the standard quantum limit, down to −6 dB. Moreover, the calculations predict entanglement between seed and conjugate beams characterized by an inseparability down to $\mathcal{I} = 0.25$. We verified that in the explored regime, the Langevin forces cannot be neglected and reduce the performances of the system. We examined the role played by the ground-state (hyperfine) coherence in the generation of quantum correlations: the smooth behavior in the low-γ region let us predict that the system is robust against mild decoherence mechanisms, as magnetic-field inhomogeneities.

Our model investigating the double-Λ scheme is quite general. It may be applied to describe a wide range of systems having the same level structure, for instance, in solid-state physics.

ACKNOWLEDGMENTS

We thank C. Fabre for enlightening discussions on the symmetrization problems related to calculations of Langevin forces. We are grateful to P. D. Lett for discussions and for providing us unpublished results that we compared against theoretical predictions. Finally, we thank P. Milman, O. Mishina, N. Sangouard, and C. Simon for fruitful discussions at the early stage of this work.

APPENDIX A: STEADY STATE

In zeroth-order perturbation expansion, in which $\hat{a}$ and $\hat{b}^\dagger$ go to zero, the Heisenberg-Langevin equations for $\hat{\sigma}_{11},\hat{\sigma}_{22},\hat{\sigma}_{33},\hat{\sigma}_{31},\hat{\sigma}_{13},\hat{\sigma}_{42},\hat{\sigma}_{24}$ atomic operators are decoupled. The mean values of these operators are required for the next-order solution. We assume the pump beam to propagate without depletion, as we verified numerically. Then the subset of equations for the mean value variables $\langle\hat{\sigma}_{11}\rangle,\langle\hat{\sigma}_{22}\rangle,\langle\hat{\sigma}_{33}\rangle,\langle\hat{\sigma}_{31}\rangle,\langle\hat{\sigma}_{13}\rangle,\langle\hat{\sigma}_{42}\rangle,\langle\hat{\sigma}_{24}\rangle$ to be solved at the steady state is written in matricial form as

$$\left(i[\mathbf{1}]\frac{\partial}{\partial t} + [\langle M_0\rangle]\right)|\Sigma_0] = |S_0], \tag{A1}$$

with

$$[M_0] = \begin{pmatrix} i\frac{\Gamma}{2} & i\frac{\Gamma}{2} & 0 & -\frac{\Omega}{2} & \frac{\Omega}{2} & 0 & 0 \\ i\frac{\Gamma}{2} & i\frac{\Gamma}{2} & 0 & 0 & 0 & -\frac{\Omega}{2} & \frac{\Omega}{2} \\ 0 & 0 & i\Gamma & \frac{\Omega}{2} & -\frac{\Omega}{2} & 0 & 0 \\ -\frac{\Omega}{2} & 0 & \frac{\Omega}{2} & -\Delta + i\frac{\Gamma}{2} & 0 & 0 & 0 \\ \frac{\Omega}{2} & 0 & -\frac{\Omega}{2} & 0 & \Delta + i\frac{\Gamma}{2} & 0 & 0 \\ -\frac{\Omega}{2} & -\Omega & -\frac{\Omega}{2} & 0 & 0 & -\Delta - \omega_0 + i\frac{\Gamma}{2} & 0 \\ \frac{\Omega}{2} & \Omega & \frac{\Omega}{2} & 0 & 0 & 0 & \Delta + \omega_0 + i\frac{\Gamma}{2} \end{pmatrix}, \tag{A2}$$

$$|\Sigma_0] = \begin{pmatrix} \sigma_{11} \\ \sigma_{22} \\ \sigma_{33} \\ \sigma_{31} \\ \sigma_{13} \\ \sigma_{42} \\ \sigma_{24} \end{pmatrix}, \quad |S_0] = \frac{1}{2}\begin{pmatrix} i\Gamma \\ i\Gamma \\ 0 \\ 0 \\ 0 \\ -\Omega \\ \Omega \end{pmatrix}. \tag{A3}$$

The steady-state solution of Eq. (A1) is

$$|\langle\Sigma_0\rangle] = [M_0]^{-1}|S_0]. \tag{A4}$$

APPENDIX B: ATOMIC HEISENBERG-LANGEVIN EQUATIONS

The first-order solution for the four coherences $\hat{\sigma}_{23},\hat{\sigma}_{41},\hat{\sigma}_{43},\hat{\sigma}_{21}$ is determined by the matricial equation

$$\left(i[\mathbf{1}]\frac{\partial}{\partial t} + [M_1]\right)|\Sigma_1] = |S_1]|\hat{A}] + i|F_1], \tag{B1}$$

with

$$[M_1] = \begin{bmatrix} i\Gamma/2 + (\Delta - \delta) & 0 & -\Omega/2 & \Omega/2 \\ 0 & i\Gamma/2 - (\Delta + \delta + \omega_0) & \Omega/2 & -\Omega/2 \\ -\Omega/2 & \Omega/2 & i\Gamma - (\delta + \omega_0) & 0 \\ \Omega/2 & -\Omega/2 & 0 & i\gamma - \delta \end{bmatrix}, \tag{B2}$$

$$|\Sigma_1] = \begin{bmatrix} \sigma_{23} \\ \sigma_{41} \\ \sigma_{43} \\ \sigma_{21} \end{bmatrix}, \quad |S_1] = g \begin{bmatrix} \langle \sigma_{33} - \sigma_{22} \rangle & 0 \\ 0 & \langle \sigma_{11} - \sigma_{44} \rangle \\ -\langle \sigma_{42} \rangle & \langle \sigma_{13} \rangle \\ \langle \sigma_{31} \rangle & -\langle \sigma_{24} \rangle \end{bmatrix}, \quad |\hat{A}] = \begin{bmatrix} \hat{a} \\ \hat{b}^\dagger \end{bmatrix}, \quad |F_1] = \begin{bmatrix} F_{23} \\ F_{41} \\ F_{43} \\ F_{21} \end{bmatrix}. \tag{B3}$$

A similar set of equations holds for the Hermitian conjugate operators.

The Langevin atomic forces $|F]$ are characterized by their diffusion coefficients matrix $[D]$ [Eq. (5)]. In order to comply with the symmetrical ordering condition introduced in Sec. V, we write the following symmetrize diffusion coefficients:

$$[D] = ([D_1] + [D_2]), \tag{B4}$$

having defined

$$[D_1] 2\delta(t - t')\delta(z - z') = \langle |F_1(z,t)][F_1^\dagger(z,t')| \rangle, \tag{B5}$$

$$[D_2] 2\delta(t - t')\delta(z - z') = \langle |F_1^\dagger(z,t)][F_1(z,t')| \rangle. \tag{B6}$$

Langevin diffusion coefficients for operators can be calculated using the *generalized Einstein relation* as in Ref. [30]. The $[D_1]$ and $[D_2]$ diffusion matrices are given by

$$[D_1] = \frac{1}{2\tau} \begin{bmatrix} \Gamma\left(\Gamma^2 + 4\Delta^2 + 2\Omega^2 + 8\Delta\omega_0 + 4\omega_0^2\right) & 0 & i\Gamma\Omega(\Gamma + 2i(\Delta + \omega_0)) & 0 \\ 0 & 0 & 0 & -i\gamma\Omega(\Gamma - 2i(\Delta + \omega_0)) \\ -i\Gamma\Omega(\Gamma - 2i(\Delta + \omega_0)) & 0 & \Gamma\Omega^2 & 0 \\ 0 & i\gamma\Omega(\Gamma + 2i(\Delta + \omega_0)) & 0 & \Gamma\Omega^2 + 2\gamma\left(\Gamma^2 + 4\Delta^2 + \Omega^2 + 8\Delta\omega_0 + 4\omega_0^2\right) \end{bmatrix}$$

$$[D_2] = \frac{1}{2\tau} \begin{bmatrix} 0 & 0 & 0 & -i\gamma(\Gamma - 2i\Delta)\Omega \\ 0 & \Gamma(\Gamma^2 + 4\Delta^2 + 2\Omega^2) & i\Gamma(\Gamma + 2i\Delta)\Omega & 0 \\ 0 & -i\Gamma(\Gamma - 2i\Delta)\Omega & \Gamma\Omega^2 & 0 \\ i\gamma(\Gamma + 2i\Delta)\Omega & 0 & 0 & \Gamma\Omega^2 + 2\gamma(\Gamma^2 + 4\Delta^2 + \Omega^2), \end{bmatrix}, \tag{B7}$$

where $\tau = 2\Gamma^2 + 4\Omega^2 + 4\omega_0^2 + 8\Delta^2 + 8\Delta\omega_0$.

The system of Eq. (B1) is solved by writing each atomic operator as the sum of its mean value and a quantum fluctuation term

$$|\Sigma_1] = |\langle \Sigma_1 \rangle] + |\delta\Sigma_1], \tag{B8}$$

By linearizing Eq. (B1) we derive for the mean values

$$|\langle \Sigma_1 \rangle] = [M_1]^{-1} |S_1] |\langle \hat{A} \rangle] \tag{B9}$$

and for the Fourier-transformed quantum fluctuations

$$|\delta\Sigma_1] = ([M_1] + \omega[\mathbb{I}])^{-1} |S_1] |\delta\hat{A}] + i([M_1] + \omega[\mathbb{I}])^{-1} |F_1]. \tag{B10}$$

APPENDIX C: QUANTUM-FIELD HEISENBERG-LANGEVIN EQUATIONS

The propagation matrix for the quantum-field operators of Eq. (11) is obtained by replacing the $\hat{\sigma}_{23}(t,z)$ and $\hat{\sigma}_{41}(t,z)$ solutions of Eq. (B8) into the differential Eqs. (6) and (7) and solving these equations. By defining

$$\begin{bmatrix} A(\omega) & B(\omega) \\ C(\omega) & D(\omega) \end{bmatrix} = e^{[M(\omega)]L}, \tag{C1}$$

where $[M(\omega)]$ is a 2×2 matrix given by

$$[M(\omega)] = -i\frac{g^2 N}{c}[T]([M_1] + \omega[\mathbb{I}])^{-1} |S_1], \tag{C2}$$

with $[T] = \left[\begin{smallmatrix} -1 & 0 & 0 & 0 \\ 0 & 1 & 0 & 0 \end{smallmatrix}\right]$.

The Langevin force terms of Eq. (11) are given by

$$\begin{bmatrix} \hat{F}_{a,\text{out}}(\omega) \\ \hat{F}_{b^\dagger,\text{out}}(\omega) \end{bmatrix} = L \int_0^1 e^{[M(\omega)]Lz} [M_F(\omega)] |F_1] \, dz, \tag{C3}$$

where

$$[M_F(\omega)] = -\frac{gN}{c}[T]([M_1] + \omega[\mathbf{1}])^{-1}. \tag{C4}$$

Let us point out that the conjugate operators for the quantum fields are given by

$$\begin{bmatrix} \delta\hat{a}^\dagger_{\text{out}}(\omega) \\ \delta\hat{b}_{\text{out}}(\omega) \end{bmatrix} = e^{[M^*(-\omega)]L} \left(\begin{bmatrix} \delta\hat{a}_{\text{in}}(\omega) \\ \delta\hat{b}^\dagger_{\text{in}}(\omega) \end{bmatrix} + \begin{bmatrix} \hat{F}_{a^\dagger,\text{out}}(\omega) \\ \hat{F}_{b,\text{out}}(\omega) \end{bmatrix} \right), \tag{C5}$$

with

$$\begin{bmatrix} F_{a^\dagger,\text{out}}(\omega) \\ F_{b,\text{out}}(\omega) \end{bmatrix} = L \int_0^1 e^{-[M^*(-\omega)]Lz} [M_F^*(-\omega)] |F_1^\dagger] dz, \tag{C6}$$

where we have introduced $|F_1^\dagger] = \begin{bmatrix} F_{32} \\ F_{14} \\ F_{34} \\ F_{12} \end{bmatrix}$.

APPENDIX D: LANGEVIN FORCES CONTRIBUTION TO NOISE SPECTRA

We will present this calculation for the $\langle \hat{F}_a(\omega)\hat{F}_{a^\dagger}(\omega')\rangle$ term, since the extension to the remaining ones is straightforward. Substituting the expression of Eq. (C6), this term is given by

$$\langle \hat{F}_a(\omega)\hat{F}_{a^\dagger}(\omega')\rangle = \langle [1\ 0| \int_0^1 e^{-[M(\omega)]Lz}[M_F(\omega)]|F_1(z,\omega)]\,dz \times \int_0^1 [F_1^\dagger(z',\omega')|\ {}^t[M_F^*(-\omega')]e^{-{}^t[M^*(-\omega')]Lz'}dz'|1\ 0]\rangle. \tag{D1}$$

The Langevin forces are δ correlated in z, so integration over z' gives

$$\langle \hat{F}_a(\omega)\hat{F}_{a^\dagger}(\omega')\rangle = [1\ 0|\left\langle \int_0^1 e^{-[M(\omega)]Lz}[M_F(\omega)]|F_1(z,\omega)] \times [F_1^\dagger(Lz,\omega')|\ {}^t[M_F^*(-\omega')]e^{-{}^t[M^*(-\omega')]Lz}\,dz\right\rangle |1\ 0]. \tag{D2}$$

By defining the $D_{aa^\dagger}(\omega)$ coefficient as

$$\langle \hat{F}_a(\omega)\hat{F}_{a^\dagger}(\omega')\rangle = D_{aa^\dagger}(\omega)2\pi\ \delta(\omega+\omega'), \tag{D3}$$

we obtain

$$D_{aa^\dagger}(\omega) = L^2[1\ 0| \int_0^1 e^{-[M(\omega)]Lz}[M_F(\omega)][D] \times {}^t[M_F^*(-\omega')]e^{-{}^t[M^*(-\omega')]Lz}dz\rangle|1\ 0], \tag{D4}$$

within the $[D]$ diffusion matrix given by Eq. (B4). In a similar way it is possible to derive $D_{a^\dagger a}(\omega)$, $D_{bb^\dagger}(\omega)$, and $D_{b^\dagger b}(\omega)$, as detailed in [45].

[1] H. P. Yuen and J. H. Shapiro, Opt. Lett. **4**, 334 (1979).
[2] R. E. Slusher, L. W. Hollberg, B. Yurke, J. C. Mertz, and J. F. Valley, Phys. Rev. Lett. **55**, 2409 (1985).
[3] M. Shahriar and P. Hemmer, Opt. Commun. **158**, 273 (1998).
[4] M. D. Lukin, P. R. Hemmer, M. O. Löffler, and M. Scully, Phys. Rev. Lett. **81**, 2675 (1998).
[5] M. D. Lukin, A. B. Matsko, M. Fleischhauer, and M. O. Scully, Phys. Rev. Lett. **82**, 1847 (1999).
[6] M. D. Lukin, P. R. Hemmer, and M. O. Scully, Adv. At. Mol. Phys. **42**, 347 (2000).
[7] A. S. Zibrov, M. D. Lukin, and M. O. Scully, Phys. Rev. Lett. **83**, 4049 (1999).
[8] M. D. Lukin and A. Imamoglu, Nature (London) **413**, 273 (2001).
[9] C. H. van der Wal, M. D. Eisaman, A. André, R. L. Walsworth, D. F. Phillips, A. S. Zibrov, and M. D. Lukin, Science **301**, 196 (2003).
[10] C. F. McCormick, V. Boyer, E. Arimondo, and P. D. Lett, Opt. Lett. **32**, 178 (2007).
[11] C. F. McCormick, A. M. Marino, V. Boyer, and P. D. Lett, e-print arXiv:quant-ph/0703111.
[12] C. F. McCormick, A. M. Marino, V. Boyer, and P. D. Lett, Phys. Rev. A **78**, 043816 (2008).
[13] R. C. Pooser, V. Boyer, A. M. Marino, and P. D. Lett, in *Quantum Communications and Quantum Imaging VI*, edited by R. Meyers, Y. Shih, and K. Deacon, *Proceedings of SPIE*, Vol. 7092 (SPIE, Bellingham, WA, 2008), 70920G-1.
[14] V. Boyer, A. M. Marino, R. C. Pooser, and P. D. Lett, Science **321**, 544 (2008).
[15] A. M. Marino, R. C. Pooser, V. Boyer, and P. D. Lett, Nature **457**, 859 (2009).
[16] Q. Glorieux, L. Guidoni, S. Guibal, J. P. Likforman, and T. Coudreau, in *Quantum Optics*, edited by V. N. Zadkov and T. Durt, *Proceedings of SPIE*, Vol. 7727 (SPIE, Brussels, Belgium, 2010), 772703.
[17] A. Kuzmich, W. P. Bowen, A. D. Boozer, A. Boca, C. W. Chou, L.-M. Duan, and H. J. Kimble, Nature **423**, 731 (2003).
[18] D. A. Braje, V. Balić, S. Goda, G. Y. Yin, and S. E. Harris, Phys. Rev. Lett. **93**, 183601 (2004).
[19] V. Balić, D. A. Braje, P. Kolchin, G. Y. Yin, and S. E. Harris, Phys. Rev. Lett. **94**, 183601 (2005).
[20] P. Kolchin, S. Du, C. Belthangady, G. Y. Yin, and S. E. Harris, Phys. Rev. Lett. **97**, 113602 (2006).
[21] P. Kolchin, C. Belthangady, S. Du, G. Y. Yin, and S. E. Harris, Phys. Rev. Lett. **101**, 103601 (2008).
[22] S. Du, P. Kolchin, C. Belthangady, G. Y. Yin, and S. E. Harris, Phys. Rev. Lett. **100**, 183603 (2008).
[23] J. K. Thompson, J. Simon, H. Loh, and V. Vuletic, Science **313**, 74 (2006).
[24] M. Fleischhauer and M. D. Lukin, Phys. Rev. Lett. **84**, 5094 (2000).
[25] C. H. R. Ooi, Q. Sun, M. S. Zubairy, and M. O. Scully, Phys. Rev. A **75**, 013820 (2007).
[26] P. Kolchin, Phys. Rev. A **75**, 033814 (2007).
[27] S. Du, J. Wen, and M. H. Rubin, J. Opt. Soc. Am. B **25**, C98 (2008).
[28] H. A. Bachor and T. C. Ralph, *A Guide to Experiments in Quantum Optics* (Wiley-VCH, New York, 2004).
[29] S. Braunstein and P. Van Loock, Rev. Mod. Phys. **77**, 513 (2005).
[30] L. Davidovich, Rev. Mod. Phys. **68**, 127 (1996).
[31] Daniel A. Steck, Rubidium 85 D Line Data, available online at [http://steck.us/alkalidata] (revision 2.1.2, 12 August, 2009).
[32] U. Schnorrberger, J. D. Thompson, S. Trotzky, R. Pugatch, N. Davidson, S. Kuhr, and I. Bloch, Phys. Rev. Lett. **103**, 033003 (2009).
[33] G. Alzetta, L. Moi, and G. Orriols, Nuovo Cimento B **52**, 209 (1979).
[34] M. Kaivola, P. Thorsen, and O. Poulsen, Phys. Rev. A **32**, 207 (1985).
[35] Yifu Zhu and T. N. Wasserlauf, Phys. Rev. A **54**, 3653 (1996).
[36] Y. Stalgies, I. Siemers, B. Appasamy, and P. E. Toschek, J. Opt. Soc. Am. B **15**, 2505 (1998).
[37] B. Lounis and C. Cohen-Tannoudji, J. Phys. II Paris **2**, 579 (1992).

[38] C. Fabre, E. Giacobino, A. Heidmann, L. Lugiato, S. Reynaud, M. Vadacchino, and Wang Kaige, Quantum Opt. **2**, 159 (1990).
[39] A. K. Ekert and P. L. Knight, Phys. Rev. A **43**, 3934 (1991).
[40] A. Heidmann, R. J. Horowicz, S. Reynaud, E. Giacobino, C. Fabre, and G. Camy, Phys. Rev. Lett. **59**, 2555 (1987).
[41] J. Laurat, T. Coudreau, L. Longchambon, and C. Fabre, Opt. Lett. **30**, 1177 (2005).
[42] Lu-Ming Duan, G. Giedke, J. I. Cirac, and P. Zoller, Phys. Rev. Lett. **84**, 2722 (2000).
[43] R. Simon, Phys. Rev. Lett. **84**, 2726 (2000).
[44] J. Laurat, G. Keller, J.-A. O. Huguenin, C. Fabre, T. Coudreau, G. Adesso, A. Serafini, and F. Illuminati, J. Opt. B **7**, S577 (2005).
[45] Q. Glorieux, Ph.D. thesis, Université Paris Diderot, 2010.